Water Research 266 (2024) 122339

Contents lists available at ScienceDirect

Water Research

journal homepage: www.elsevier.com/locate/watres

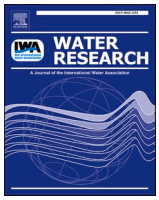

Wind and rain compound with tides to cause frequent and unexpected coastal floods

Thomas Thelen [a,*], Katherine Anarde [a], Joel Casey Dietrich [a], Miyuki Hino [b,c]

[a] Department of Civil, Construction, and Environmental Engineering, North Carolina State University, 915 Partners Way, Raleigh, NC, USA
[b] Department of City and Regional Planning, University of North Carolina at Chapel Hill, 223 E Cameron Avenue, Chapel Hill, NC, USA
[c] Environment, Ecology, and Energy Program, University of North Carolina at Chapel Hill, 121 South Road, Chapel Hill, NC, USA

ARTICLE INFO

Keywords:
Coastal flooding
Sea-level rise
High-tide flooding
Compound flooding
Hydrodynamic modeling
Climate adaptation

ABSTRACT

With sea-level rise, flooding in coastal communities is now common during the highest high tides. Floods also occur at normal tidal levels when rainfall overcomes stormwater infrastructure that is partially submerged by tides. Data describing this type of compound flooding is scarce and, therefore, it is unclear how often these floods occur and the extent to which non-tidal factors contribute to flooding. We combine measurements of flooding on roads and within storm drains with a numerical model to examine processes that contribute to flooding in Carolina Beach, NC, USA – a community that chronically floods outside of extreme storms despite flood mitigation infrastructure to combat tidal flooding. Of the 43 non-storm floods we measured during a year-long study period, one-third were unexpected based on the tidal threshold used by the community for flood monitoring. We introduce a novel model coupling between an ocean-scale hydrodynamic model (ADCIRC) and a community-scale surface water and pipe flow model (3Di) to quantify contributions from multiple flood drivers. Accounting for the compounding effects of tides, wind, and rain increases flood water levels by up to 0.4 m compared to simulations that include only tides. Setup from sustained (non-storm) regional winds causes deeper, longer, more extensive flooding during the highest high tides and can cause floods on days when flooding would not have occurred due to tides alone. Rainfall also contributes to unexpected floods; because tides submerge stormwater outfalls on a daily basis, even minor rainstorms lead to flooding as runoff has nowhere to drain. As a particularly low-lying coastal community, Carolina Beach provides a glimpse into future challenges that coastal communities worldwide will face in predicting, preparing for, and adapting to increasingly frequent flooding from compounding tidal and non-tidal drivers atop sea-level rise.

1. Introduction

As sea levels continue to rise, coastal floods are occurring more frequently even in the absence of extreme storms (Sweet et al., 2022). Marine water levels overtop low-lying shorelines and backflow into stormwater infrastructure (pipes and ditches) during the highest high tides, flooding roads and other low-lying areas (Sweet et al., 2018). Flooding also occurs during normal tidal levels due to impaired stormwater infrastructure: with reduced capacity to convey runoff, everyday rainstorms can overcome submerged or partially full stormwater networks, leading to flash floods (Gold et al., 2023; Sadler et al., 2020). Sea-level rise (SLR) has also elevated shallow groundwater tables, reducing infiltration of rainfall runoff on the surface and increasing rates of infiltration into stormwater drainage networks in the subsurface (Befus et al., 2020; Bosserelle et al., 2022). These land-based drivers complicate the usage of terminology used to describe flooding from SLR (e.g., “high-tide flooding” or “sunny-day flooding”). Here, we use the terms “chronic coastal flooding” (Hague et al., 2023) or “chronic flooding” (Thiéblemont et al., 2023), to include all recurrent coastal floods occurring outside of extreme storms (i.e., named tropical storms and Nor’easters) due to both marine (e.g., tides, wind, atmospheric pressure) and land-based drivers (e.g., rain, impaired stormwater networks, groundwater) acting atop higher sea levels.

Evidence of the frequency, spatial extent, and mechanisms driving chronic coastal flooding is scarce. Due to data availability, previous work has largely focused on contributions to floods from marine sources. Analysis of tide gauge data has shown that ocean-scale processes like wind setup, circulation patterns, and thermal expansion combine with

* Corresponding author.
E-mail addresses: ththelen@ncsu.edu (T. Thelen), kanarde@ncsu.edu (K. Anarde), jcdietrich@ncsu.edu (J.C. Dietrich), mhino@unc.edu (M. Hino).

https://doi.org/10.1016/j.watres.2024.122339
Received 10 June 2024; Received in revised form 19 August 2024; Accepted 25 August 2024
Available online 28 August 2024

tides to elevate water levels along the coast (Li et al., 2022). These "non-tidal residuals" contribute significantly to marine water levels during high-tide floods along the East Coast of the United States (Li et al., 2022), and are incorporated in high-tide flood predictions made at tide gauges (Dusek et al., 2022). Tide gauges, however, are geographically sparse. They are also located over marine water bodies and therefore cannot capture localized, land-based flood drivers, which cause variations in flooding on the scale of city blocks (Shen et al., 2019). Flood data from in-situ sensors on land have been limited in space and time, restricted to a few communities and characterized by short time records (Gold et al., 2023; Mydlarz et al., 2024; Silverman et al., 2022). More data and new methods are needed to quantify the relative importance of land and marine-based flood drivers to chronic coastal floods at a block-by-block scale.

The most common approach for investigating the spatial extent and depth of chronic coastal flooding is "bathtub" modeling, where all elevations below a given water level are considered inundated (e.g., Gold et al., 2022; Williams and Lück-Vogel, 2020; Yunus et al., 2016). Because this method combines all flood drivers into one total water level term, it cannot resolve interactions between multiple flood drivers, nor interactions with infrastructure, which cause more complex flood patterns. In contrast to bathtub modeling, combined surface water and pipe flow models capture interactions between land and marine-based drivers. Numerical models that couple 1D pipe flow simulations and 2D surface flow simulations are used to simulate multi-driver flooding in urban areas (e.g., Fan et al., 2017; Seyoum et al., 2012). However, their application to coastal flooding is less common (Sadler et al., 2020; Shen et al., 2019; Zahura and Goodall, 2022). While 1D-2D models of chronic coastal flooding have the potential to resolve multiple flood drivers interacting with infrastructure, model results in coastal systems have not been validated against direct measurements of flooding on land, nor have the models been adapted to analyze the contributions of flood drivers acting over multiple spatial scales (e.g., rainfall runoff within a city block versus wind setup acting over a long fetch).

A growing body of literature has identified impacts of chronic coastal floods to people, businesses, and communities, with impacts spanning traffic delays (Hauer et al., 2023), water quality risks (Macías-Tapia et al., 2021; Carr et al., 2024), reduced economic activity (Hino et al., 2019), property damage (Moftakhari et al., 2018), and changing development patterns (Buckman and Sobhaninia, 2022). Given the limited data describing this type of flooding and the lack of validated models capable of resolving flood drivers at relevant spatial and temporal scales, relating impacts to flood mechanisms remains difficult, constraining our understanding of the social and economic burden of these floods. Uncertainty in the relative importance of tidal versus non-tidal flood drivers also hampers flood prediction and community preparedness for floods, particularly in regions far from tide gauges.

We combine land-based flood measurements with a new coupled hydrodynamic and stormwater model to examine variability in processes that drive chronic flooding in a coastal community over seasonal timescales, and relate this understanding to how communities prepare for flooding outside of extreme storms. Our analysis focuses on the Town of Carolina Beach, North Carolina (NC), USA, a coastal community that employs preventative infrastructure and flood monitoring thresholds to try to minimize impacts from chronic flooding. We find that one-third of measured floods occurred at forecasted tides below the community's flood monitoring threshold because of contributions from wind, rain, and impaired stormwater networks. We place our findings in context of how low-lying coastal communities may use local knowledge of the relative importance of different flood drivers to better prepare for current and future flood hazards.

2. Methods

2.1. Study location

The Town of Carolina Beach sits between the Cape Fear River Estuary to the west and the Atlantic Ocean to the east (Fig. 1A). North of Carolina Beach, these two water bodies connect via a man-made waterway (Snow's Cut, part of the Intracoastal Waterway) and a tidal inlet. The Yacht Basin is a dredged back-bay that extends south into Carolina Beach from the Intracoastal Waterway. Flooding occurs regularly on Canal Drive, a low-lying road running along reclaimed land on the eastern edge of the Yacht Basin (Fig. 1B). During these chronic flood events, water from the Yacht Basin propagates up through subterranean stormwater infrastructure to flood the road, often prior to the overtopping of bay shorelines and bulkheads.

The Town of Carolina Beach has sought to mitigate flooding emanating from the stormwater system through installation of backflow prevention devices on stormwater outfalls to the Yacht Basin located at each intersection along Canal Drive (e.g., Fig. 1C). These devices include inline check valves and external "duckbill" devices designed to allow only one-way flow; when functioning as intended, these devices prevent water from entering the stormwater system from the Yacht Basin during high water levels while allowing water to exit the pipes during low water levels. The Town's stormwater network is disconnected, so backflow prevention from each of these devices is localized to clusters of catch basins and pipes that drain individual intersections (e.g., Fig. 1C).

Individual homeowners also employ localized flood mitigation through construction of bulkheads. Bulkheads along Canal Drive vary in elevation and are not continuous. A 2019 Flooding and Vulnerability Study (APTIM, 2019) documented bulkheads installed on 89 % of the 144 lots surrounding the Yacht Basin. However, it is unclear how much flooding along Canal Drive stems from overtopping of low-lying shorelines (around/over bulkheads) compared to the failure of backflow prevention devices (due to biofouling, debris, or groundwater bypassing).

Town of Carolina Beach staff regulate access to Canal Drive during floods through a series of gates restricting access to the road. Decisions to monitor the roadway or close the gates are made using local forecasts of peak astronomical tides. If the forecasted tide exceeds 1.83 m (6 ft) Mean Lower Low Water (MLLW) the gates are lowered. These highest high tides occur during, for example, perigean spring tides, when the moon, earth, and sun are in alignment, and the moon is closest in its orbit to earth. If the forecasted tide is between 1.83 and 1.60 m MLLW, Town staff monitor Canal Drive in person and close the road if flooding is observed. Canal Drive is not proactively monitored if the forecasted tide is less than 1.60 m (5.25 ft) MLLW, except when strong northerly winds are forecast which Town staff know anecdotally can elevate water levels in the Yacht Basin. Despite local knowledge of the importance of wind to flooding, there are currently no thresholds for wind intensity or direction included in Town decision-making for road closures. This is largely due to a lack of information on non-tidal drivers tailored to the needs of Town staff. In the following sections, we describe a two-pronged approach – developed in collaboration with Town officials – which combines measured data and numerical modeling to improve understanding of factors that lead to flooding.

2.2. In-situ measurement of flood incidence and extent

We worked with Town officials to instrument flood hotspots along Canal Drive with Sunny Day Flooding Sensors (SuDS; Gold et al., 2023). Each SuDS installation consists of a pressure sensor installed in a stormwater catch basin and a co-located sub-aerial gateway with a camera. Collectively, the sensors transmit water levels and roadway images every six minutes to a web application, which serves as a real-time indicator for the Town of flood incidence and spatial extent (Hayden-Lowe et al., 2022). The sensors were validated through

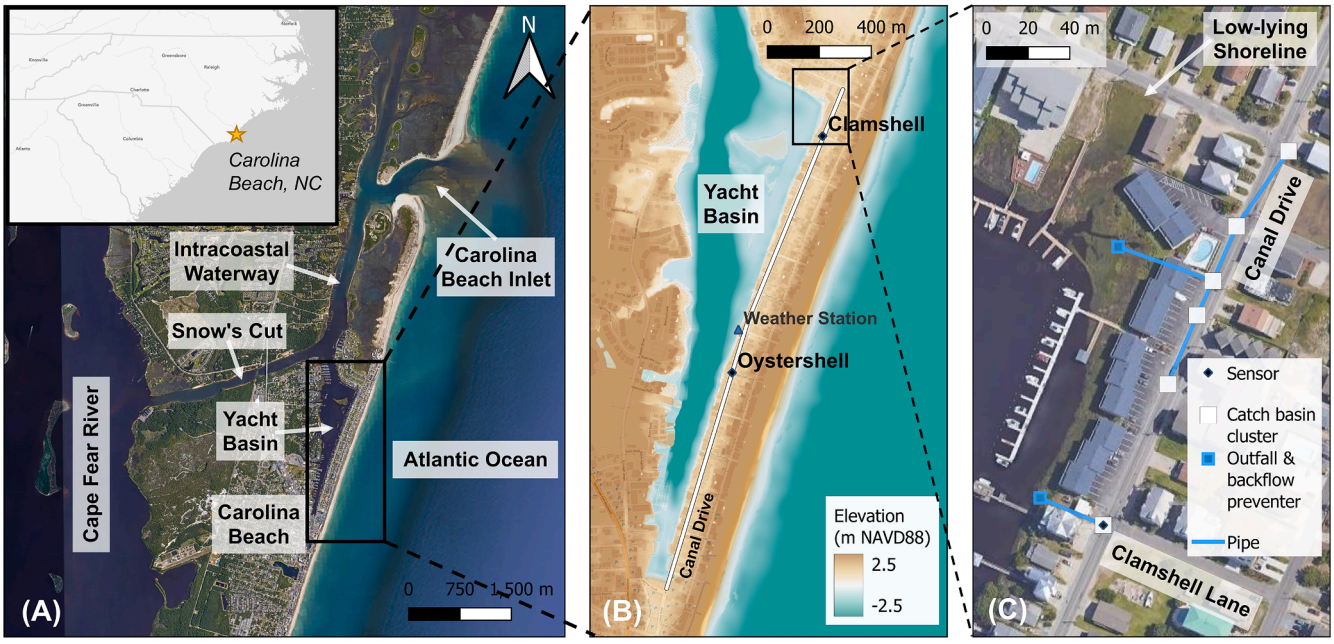

Fig. 1. (A) Carolina Beach study site and neighboring water bodies. (B) Elevation map (Coastal National Elevation Database; Thatcher et al., 2016) of the study site (black box in A), including the location of Clamshell Lane and Oystershell Lane flood sensors that measure water levels and collect images of flood extent along Canal Drive (black diamonds) and the Town-operated weather station (blue triangle). (C) Zoomed-in view of the stormwater infrastructure along the north end of Canal Drive (black box in B). The stormwater infrastructure at all other cross-streets intersecting Canal Drive is similar to the Clamshell Lane intersection with Canal Drive in (C), where clusters of catch basins drain directly to the Yacht Basin without any additional subterranean (pipe) connections along Canal Drive.

comparison with an in-situ commercial water level sensor (Supplementary Fig. S.9).

This paper uses data from the two sensors with the longest data records: the sensor at the intersection of Canal Drive and Clamshell Lane, and the sensor at the intersection of Canal Drive and Oystershell Lane (Fig. 1B; referred to as the "Clamshell" and "Oystershell'' sensors). Measurements span April 1, 2022 to April 24, 2023 at the Clamshell sensor and June 2, 2022 to April 24, 2023 at the Oystershell sensor. Intermittent sensor outages occurred due to issues with batteries and sensor housing leaks. Water levels were recorded for 76 % of the study periods at the two sensors (Supplementary Table S.3). There were fewer data gaps in the imagery record; we recorded images for 95 % of the study period at the Clamshell location and 99 % of the study period at the Oystershell location.

We use the in-situ water levels and camera imagery to assess flood incidence and to validate the numerical model. We define a flood as occurring when water levels surpass the elevation of the top of the catch basin grate, which are immediately adjacent to the road at both sensor locations. We consider any amount of water on the road as a potential flood impact because even small puddles of saltwater can splash onto the underside of vehicles and cause corrosion. For our analysis, a flood ends when water levels recede below the top of grate elevation. Flood magnitude is calculated as the maximum water depth above the edge of the road.

2.3. Wind and rain measurements

A weather station in the Yacht Basin (Fig. 1B) records 10-minute wind speed and direction, and rain accumulation measured every minute. It also records water levels in the Yacht Basin at intervals of no longer than 10 min. Wind speeds measured at the station are lower than what would be measured on the open coast because the Yacht Basin is ringed by structures that block wind. Wind speed and direction associated with a flood are averaged over the 24 h preceding each event because sensitivity testing with different averaging intervals shows this interval balances over-smoothing longer-term changes in wind direction with misrepresenting shorter-term changes in wind speed. To calculate the rain accumulation associated with a flood, we consider the duration of the flood and the two hours prior, thereby capturing the upper half of the rising tide that inundates stormwater outfalls and impedes drainage.

2.4. Multi-driver flood model

Data on flood incidence and depth are used to validate a numerical model capable of simulating water level contributions from multiple drivers. The flood model consists of an ocean-scale circulation model that is one-way coupled to a community-scale flood model. Collectively, the coupled model can simulate tides, atmospheric conditions (air pressure and wind), rainfall runoff, pipe flow, surface water flow, and the effects of infrastructure like backflow prevention devices and bulkheads. In the sections that follow, we summarize model components and coupling.

2.4.1. Ocean-scale circulation model: ADCIRC

We use the Advanced Circulation Model (ADCIRC; Luettich et al., 1992; Westerink et al., 1992) to simulate offshore and nearshore drivers of coastal water levels. ADCIRC uses unstructured meshes to represent complex coastal environments and predict the effects of tides, winds, and river flows on water levels and depth-averaged currents. Our ADCIRC simulations are performed using the NC Coastal Flood Analysis System Model Grid (Blanton and Luettich, 2008), which covers the Western North Atlantic Ocean. The mesh was designed for floodplain mapping and storm surge prediction in NC; therefore, its highest resolution is along the NC coast and surrounding floodplains (approx. 40 m to 150 m). To improve the representation of topography and bathymetry near our study site, we interpolated elevations reported in the Coastal National Elevation Database (CoNED; Thatcher et al., 2016 – vertical accuracy of 0.35 m) to the ADCIRC mesh around Carolina Beach.

Tides with four diurnal (K1, O1, P1, and Q1) and semidiurnal (M2, S2, N2, and K2) constituents are applied as periodic forcing at the open ocean boundary and as potentials throughout the model domain. Atmospheric forcing consists of wind speed and air pressure data from the

North American Mesoscale (NAM) Forecast System Analysis product (Rogers et al., 2009) interpolated at three-hour intervals from the 12-km NAM product grid to the ADCIRC mesh. All simulations include a seven-day ramp for tidal and atmospheric forcings.

Lastly, we set a global water level offset in ADCIRC to account for seasonal water level fluctuations that are not captured in the atmospheric forcing (e.g., thermal expansion – Asher et al., 2019). This offset was calculated by comparing model output prior to a flood with measurements of water levels from the Yacht Basin weather station (Supplementary Eq. S.1).

2.4.2. Community-scale flood model: 3Di

We couple ADCIRC with the hydrodynamic model 3Di (Stelling, 2012) to simulate land-based flood drivers, including pluvial flooding (i.e., rainfall) and the effects of stormwater infrastructure (i.e., pipe networks and backflow prevention devices). 3Di simulates one-dimensional pipe flows (Casulli and Stelling, 2013), two-dimensional surface water flows (Casulli, 2009; Casulli and Stelling, 2011), and their interactions, resulting in a mass-conservative simulation of free surface and pipe flows. 3Di has been used previously to map SLR and storm inundation (Ju et al., 2017). This is the first coupling of 3Di with ADCIRC.

The 3Di model domain includes the land and waterways in and around Carolina Beach (area within the white and orange outlines in Fig. 2). The 3Di subgrid calculation method enables calculated water depths to vary at the resolution of the input elevation raster (Casulli and Stelling, 2011; Volp et al., 2013) such that simulated flood extents and depths reflect small variations in topography. We use the 1-m horizontal resolution CoNED digital elevation model (Thatcher et al., 2016) as the elevation raster input for 3Di. The calculation grid resolution is shown in Fig. 2, with the highest resolution (12 m) in the Yacht Basin, nearby channels, nearshore ocean, and along Canal Drive. The calculation grid scales out to a 24-m resolution in the inlet and back-bay waterways far from the Yacht Basin, and a 192-m resolution in the open ocean far from the inlet. Bottom friction is represented with Manning's n values converted from a land-cover data set (Dietrich et al., 2011; Office for Coastal Management, 2022). Pluvial contributions to flooding are simulated using five-minute rainfall measured at the weather station (Fig. 1B) applied as a spatially constant input. Because the study area is heavily developed with extensive impervious or low-infiltration surfaces and the groundwater table is high in low-lying coastal areas (Bosserelle et al., 2022), we assume no infiltration in 3Di simulations.

Stormwater infrastructure along Canal Drive is represented in 3Di by 1D flow features. Each inlet cluster at a Canal Drive intersection is modeled using a single catch basin node at the lowest point of the 12 m calculation cell. Bulkheads are modeled as linear obstacles, with elevations sourced from the Flooding and Vulnerability Study (APTIM, 2019). To simulate the effect of backflow prevention devices in the subterranean pipe network, we apply 1D weir equations at the outfall from the catch basin nodes to the Yacht Basin. This is a similar approach to Gallegos et al., (2009) and Schubert et al., (2024) who used 1D weir equations to simulate flow through curb inlets during urban floods. Here, we tune the discharge coefficients in the weir equations (Supplementary Eqn. S.2) to best match the hydrographs measured by the in-situ flood sensors (Supplementary Fig. S.4). This parameterization of the backflow prevention devices incorporates site-specific processes because our measured water levels in the catch basins are influenced by 1) processes that reduce the effectiveness of the backflow prevention devices, like biofouling; and 2) infiltration of groundwater via cracks in the stormwater network.

2.4.3. Model coupling

The coupling between ADCIRC and 3Di is one-way, meaning that ADCIRC water levels are boundary conditions for the 3Di model. Two-minute interval water level time series interpolated from ADCIRC

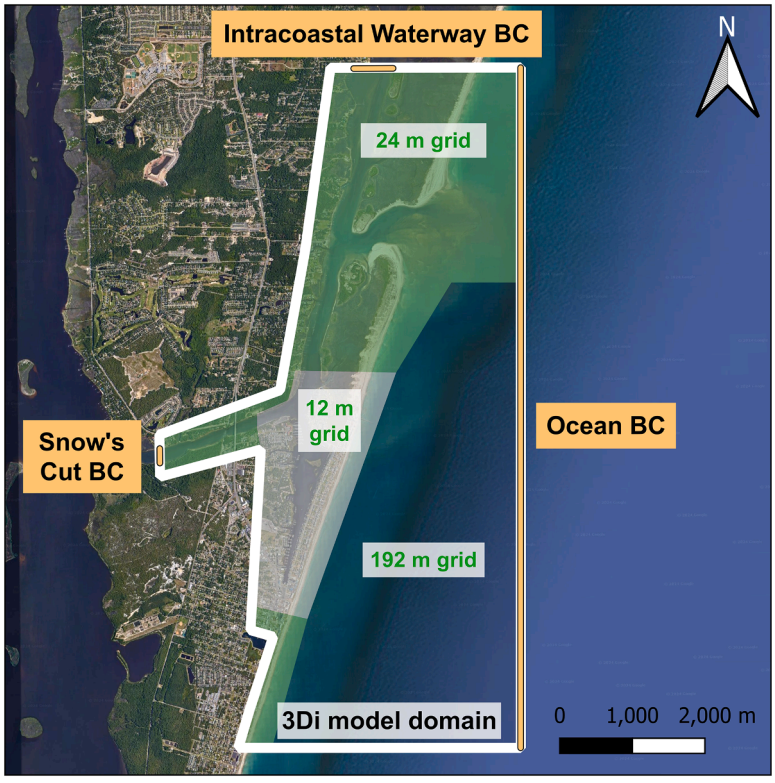

Fig. 2. 3Di model domain and grid resolution. The extents of the 3Di model domain are shown in white, and the boundaries used for the one-way coupling from ADCIRC to 3Di at the edges of the 3Di model domain are shown in orange. Shaded areas show the different grid resolutions within the 3Di model domain: 12 m around the Yacht Basin, 24 m around back-bay waterways and the inlet, and 192 m in the open ocean far from the inlet. 3Di uses elevations from the Coastal National Elevation Database (Thatcher et al., 2016) stored in the model subgrid to calculate water depths that vary at 1-m horizontal resolution.

force surface water flows at the 3Di model boundaries (orange lines in Fig. 2). The final simulation product from the coupled "flood model" are water depths resolved at a six-minute temporal resolution and one-meter spatial resolution on land and within subterranean stormwater infrastructure.

2.5. Modeled decomposition of flood drivers

We developed the flood model to better understand the relative contributions of tides, atmospheric conditions, and rainfall to total water levels on land and in stormwater infrastructure during flood events. We compare three model simulations for each hindcast flood event, with each simulation incorporating additional forcing. The first model simulation includes only tidal forcing (referred to as the "tides'' simulation). The second model simulation includes both tidal and atmospheric forcings from ADCIRC, including the effects of pressure and wind (the "tides + atmospheric" simulation). The third simulation includes three forcings: tides and atmospheric forcing in ADCIRC plus rainfall in 3Di (the "tides + atmospheric + rainfall" simulation). Water levels from the tides + atmospheric + rainfall simulation are compared to measured water levels at the Clamshell and Oystershell catch basins for three hindcast flood events (Table 2) for model validation. The influence of individual flood drivers is then found by differencing these model simulations as shown by the driver decomposition formulations in Table 1.

3. Results

3.1. Flood measurements and community response

From April 1, 2022 to April 24, 2023, we recorded 56 instances of water levels above the roadway in Carolina Beach (at the Clamshell sensor, Fig. 1, which is the longest data record). Ten floods identified using imagery alone are excluded from Fig. 3 because we do not have water level measurements due to pressure sensor outages. We also exclude three floods that occurred during Hurricane Ian (September 29-30, 2022; Fig. 3A), the only named storm that made landfall in the mid-Atlantic during the study period. As in Gold et al. (2023), we categorize the remaining 43 chronic floods as "rainy-day" floods – that is, floods that coincided with a rain event – or "sunny-day" floods – floods that occurred with no measured precipitation. Using this nomenclature, we observed 28 sunny-day floods (Fig. 3B, yellow circles) and 15 rainy-day floods (Fig. 3B, teal triangles). Rain accumulation varied from 0.2 mm to 37.6 mm (Fig. 3B, size of teal triangles). We find that rainy-day floods were typically longer in duration, for the same flood magnitude, than sunny-day floods.

Over the study period, 33 % of chronic floods (14 of 43 floods) occurred during forecasted tides below the Town's monitoring threshold, meaning these floods were largely unexpected (Fig. 3C). Comparison of tidal and meteorological data indicates that all 14 unexpected floods occurred during a rising or high tide accompanied by northeasterly winds, rainfall, or a combination of the two (Fig. 3D). Eleven of the 14 unexpected floods occurred during a northeasterly wind (orange circles and triangles in the upper right quadrant of Fig. 3D), with wind speeds ranging from 2.2 m/s to 6.8 m/s (averaged over the 24 h preceding the event). Of the 11 unexpected floods concomitant with a northeasterly wind, four were also accompanied by rainfall. The remaining 3 unexpected floods that occurred without northeasterly winds were concomitant with rainfall (orange triangles, lower half of Fig. 3D).

The largest flood magnitudes (i.e., maximum depth at the sensor location) occurred when wind was northeasterly. For the six largest floods – the floods that exceed the 0.4-m radial axis line in Fig. 3D, which corresponds to flood magnitude – the same number occurred during high tidal stages (black dot) and low tidal stages (orange triangle, denoting rain and northeasterly wind).

Table 1
Formulations used to decompose modeled water level contributions from tides, atmospheric conditions, and rainfall during hindcast flood events.

Flooding driver	Water level time series decomposition to isolate driver contribution
Tides	(tides simulation)
Atmospheric conditions	(tides + atmospheric simulation) *minus* (tides simulation)
Rainfall	(tides + atmospheric + rainfall simulation) *minus* (tides + atmospheric simulation)

3.2. Flood modeling and driver decomposition

We use the flood model to quantify contributions of individual flood drivers to flood magnitude, duration, and spatial extent for three measured flood events. These floods (points with white centers in Fig. 3D) span different combinations of tidal and meteorological conditions, as well as community preparedness. Table 2 summarizes the forecasted tidal levels (i.e., used for monitoring and closing roads), actual community response (i.e., alerts and road closures), measured rain accumulation, and measured wind speed and direction for each flood. We refer to these flood events by the month and year that they occurred, and the hypothesized primary flood driver.

The "June 2022 perigean spring tide event" included two floods (June 14-15 and 15-16) during perigean spring tides. These floods co-occurred with the second (June 14-15) and fourth (June 15-16) highest forecasted tidal peaks of the year (NOAA, 2022). The community was alert to flooding during this event, as evidenced by pre-emptive road closures on Canal Drive and a "king tide" flood alert post on Facebook. Conversely, the "August 2022 rain event" occurred during one of the smallest forecasted tidal peaks of the month (NOAA, 2022). Road closure barriers were not placed on Canal Drive before or during this flood event, nor was there a social media alert. The forecasted tide during the "January 2023 mixed-drivers event" was higher than the August event but lower than the June event, within the monitoring range for road closure. For this event, barriers were placed on Canal Drive 30 min before the flood, but there was no social media alert. Imagery from the flood sensors during each event is included in the Supplement (Fig. S.5-8).

In the sections that follow, we examine three simulations for each modeled flood event using the forcing combinations identified in Table 2: tides, tides + atmospheric, and tides + atmospheric + rainfall. First, we compare in-situ sensor data and modeled water levels from each event. Then, we examine trends spatially.

3.2.1. June 2022 perigean spring tide event

During the June 2022 perigean spring tide event, two floods were measured during the highest high tides each day (dotted black lines in Fig. 4B): a smaller flood on the evening of June 14 (black dot with white interior in the lower left quadrant of Fig. 3D) and a larger flood on the evening of June 15 (black dot with white interior in the upper right quadrant of Fig. 3D). (At this time, the Oystershell sensor had not yet been installed, so only the Clamshell sensor is shown in Fig. 4). The measured water level time series for this event demonstrates how high water levels in the Yacht Basin – in the absence of rain – can cause flooding on Canal Drive. As bay water levels increase with a rising tide, stormwater outfalls become inundated, but backflow prevention devices slow the flow of bay water into the stormwater system (shown in Fig. 4B by the gradual increase in slope of the dotted line at the beginning of each rising tide). The Clamshell catch basin fills rapidly once water levels surpass the lowest-lying shoreline along the perimeter of the Yacht Basin and flow overland to Canal Drive; this phenomenon is visible in imagery and manifests in the measured water level time series by sudden increases in water level at 21:00 on June 14 and June 15.

The model indicates that atmospheric forcing contributed to

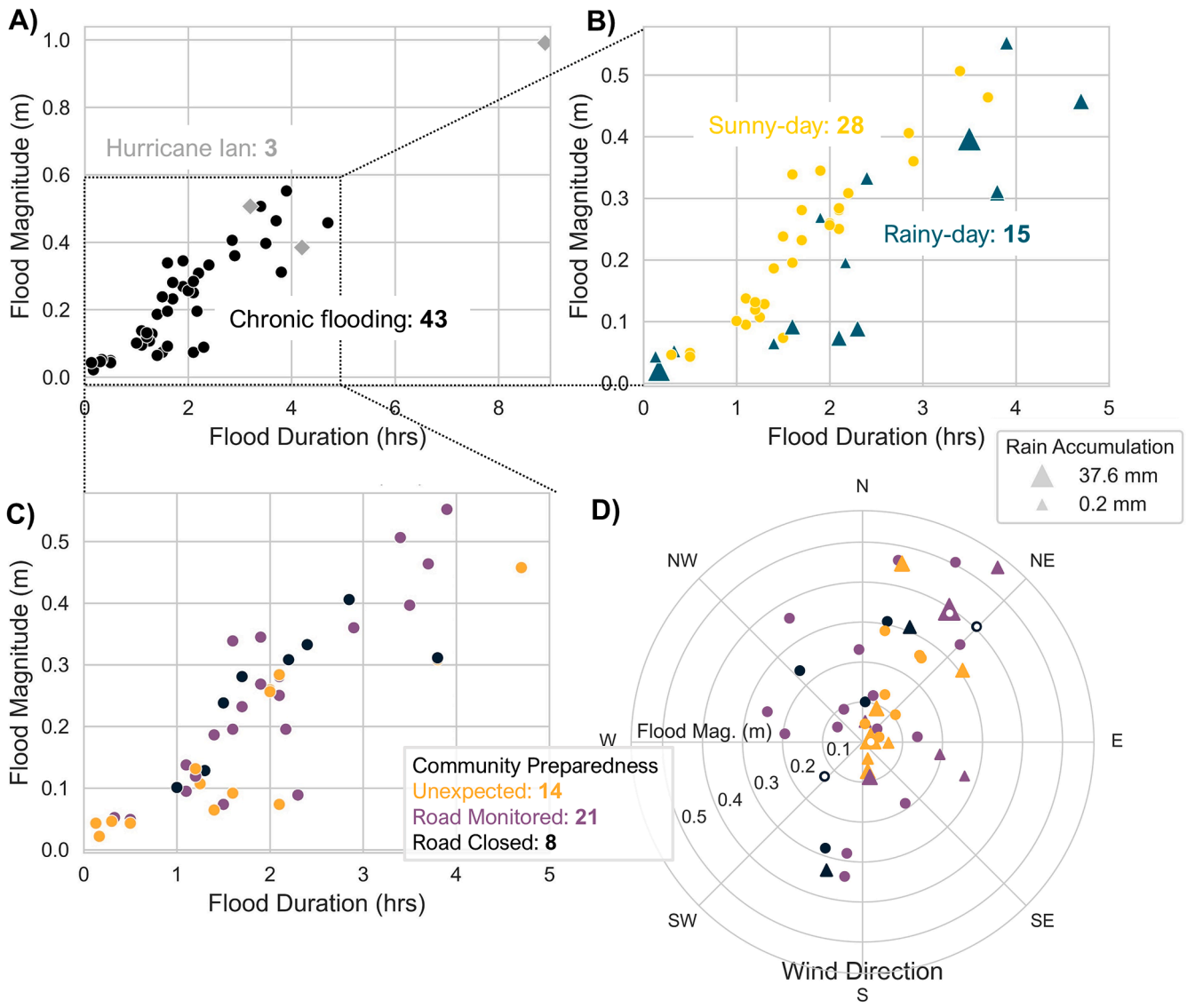

Fig. 3. In-situ measurements of flood magnitude (maximum water depth on road) at the Clamshell sensor (Fig. 1, April 1, 2022 - April 24, 2023), plotted against flood duration (A-C) and wind direction (D). (B-D) examine only the "chronic floods" (black dots in A) that occurred outside of named extreme storms (gray diamonds in A). In (B), floods are classified as sunny-day floods (yellow circles) or rainy-day floods (teal triangles, where size scales with the magnitude of rain accumulation during the flood and the two preceding hours). In (C), floods are binned by the level of community preparedness for the flood: black indicates preemptive road closure (forecasted tide $\geq$ 1.83 m MLLW), purple indicates monitoring of road conditions (tide between 1.60 and 1.83 m MLLW), and orange indicates "unexpected" floods when the road was not monitored or closed based on tidal forecasts (tide $<$ 1.60 m MLLW). In (D), wind direction (where the wind was blowing from) is averaged over the 24 h preceding the flood; the radial axis shows flood magnitude; the scaling of triangles shows rain accumulation as in (B); the point coloring shows community preparedness as in (C); and flood points with white interiors are modeled in Section 3.2.

roadway flooding during the June 2022 perigean spring tide event. Comparison of the tides + atmospheric and tides simulations show that regional atmospheric conditions (Supplementary Section 8) reduced water levels (i.e., setdown) until the evening of June 15 (Fig. 4C, shown through a shift in atmospheric water level contributions from negative to positive). Thereafter, a change in wind direction – from southwesterly to northeasterly (Fig. 4A) – elevated water levels (i.e., setup) across the continental shelf (Supplementary Fig. S.10) and in the Yacht Basin (Supplementary Fig. S.1) by about 0.1 m, which when combined with tides, resulted in more flooding on the road (Fig. 4B). The flood model reproduces overland flooding at the Clamshell catch basin for the June 15-16 flood (Fig. 4B, rapid increase in the solid pink and dashed purple lines at 21:00 on June 15) but not for the June 14-15 flood, as modeled water levels in the Yacht Basin for the tides + atmospheric simulation were 0.1 m lower than measured water levels at the flood peak (see Supplementary Fig. S.1).

3.2.2. *August 2022 rain event*

Flooding during the August 2022 rain event was unexpected based on tidal forecasts. Before and after the flood event, backflow prevention devices limited the amount of bay water entering the stormwater network at Clamshell Lane and Oystershell Lane during each high tide (Fig. 5B and D, respectively). On August 19, a rainfall event occurred during the rising tide (33 mm over two-hours, Fig. 5A). This event was a typical rainstorm; it was smaller than the one-year average recurrence interval for two-hour precipitation at Carolina Beach (56 mm; Bonnin et al., 2004). Flood depths on the roadway were small at both sensor locations ($<$0.2 m), but were larger at Oystershell Lane, which is higher in elevation.

Model simulations show the August 2022 rain event was driven by rainfall. Neither tides nor tides + atmospheric contributions elevated water levels in the Yacht Basin enough to flood the road at Clamshell (Fig. 5C) or Oystershell (Fig. 5E) Lane. However, the tides +

Table 2
The three measured flood events selected for modeling. The names associated with each flood event include the month that they occurred and the hypothesized primary flood driver.

Modeled flood events	June 2022 perigean spring tide event	August 2022 rain event	January 2023 mixed-drivers event
Flood date or dates	June 14-16	August 19	January 22
Predicted high tide (m MLLW)	1.92 m	1.37 m	1.77 m
Community preparedness measures	Pre-emptive social media post, road closure	None	Road closure as flooding started
Measured rain accumulation	None	33 mm over 2 h	48 mm over 6 h
Measured wind speed and direction	June 14-15: 3.3 m/s, 230°N June 15-16: 2.2 m/s, 40°N	1.9 m/s, 70°N	2.5 m/s, 30°N

atmospheric simulation shows that there was reduced capacity in both catch basins during the rainfall event due to the rising tide, impairing drainage of rainfall runoff to the Yacht Basin (Fig. 5B,D). The differing flood magnitudes and durations at the two sensor locations stem from a combination of differences in rainfall runoff draining to each catch basin (i.e., differences in tributary area and the amount of impervious surfaces) and differences in stormwater capacity (i.e., how bay water impedes drainage through the network).

3.2.3. *January 2023 mixed-drivers event*

On the morning of January 22, 2023, the Clamshell and Oystershell sensors measured floods that reached 0.4 m in magnitude and 4 h in duration (Fig. 6B,D), which were the largest and longest floods of the three events examined through modeling. Prior to the flood, a low-pressure system located offshore Carolina Beach began moving north past the study site (Weather Forecast Office, 2023), producing a shift in wind from southwesterly to northeasterly at 00:00 on January 21 (Fig. 6A). Approximately 24 h later, on the morning of January 22, the offshore low produced a 48-mm, six-hour rain event (Fig. 6A). Like the August 2022 rain event, this rainfall event was a relatively typical rainstorm; the one-year average recurrence interval for six-hour precipitation in Carolina Beach is 75 mm (Bonnin et al., 2004).

Model simulations indicate that flooding would not have occurred at either sensor location during the January 2023 mixed-drivers event due to tides alone (Fig. 6B,D, pink line); only after incorporation of regional atmospheric effects (Supplementary Section 8) and rain do simulation results approach the observed 0.4 m flood magnitude (Fig. 6B,D, dash-dot blue line compared to dotted black line). Decomposition of atmospheric contributions show that southwesterly winds prior to arrival of the offshore low produced a setdown of water levels in the Yacht Basin (Fig. 6C,E, negative purple dashed line) through January 20. With the arrival of the offshore low on January 21-22 and associated shift in wind direction, atmospheric contributions to water levels reversed from negative to positive across the continental shelf (regional setup between 0.1 and 0.2 m; Supplementary Fig. S.11), in the Yacht Basin (Supplementary Fig. S.3), and at both catch basins (i.e., at 06:00 on Jan. 22 in Fig. 6C,E). Thereafter, tides compounded with atmospheric effects to first reduce, and later eliminate, drainage capacity in the stormwater system. At both sensor locations, the tide filled the Yacht Basin to near to the elevation of the outfall (Fig. 6B,D, pink line). Rainfall commenced thereafter, and with reduced capacity in the stormwater network, runoff overwhelmed the system and flooded the road (Fig. 6B,D, blue dash-dot line). Rainfall contributions to water levels (above the outfall elevation) were largest at both locations at this time (Fig. 6C,E, dash-dot blue line). Thereafter, the combined influence of atmospheric effects and rising

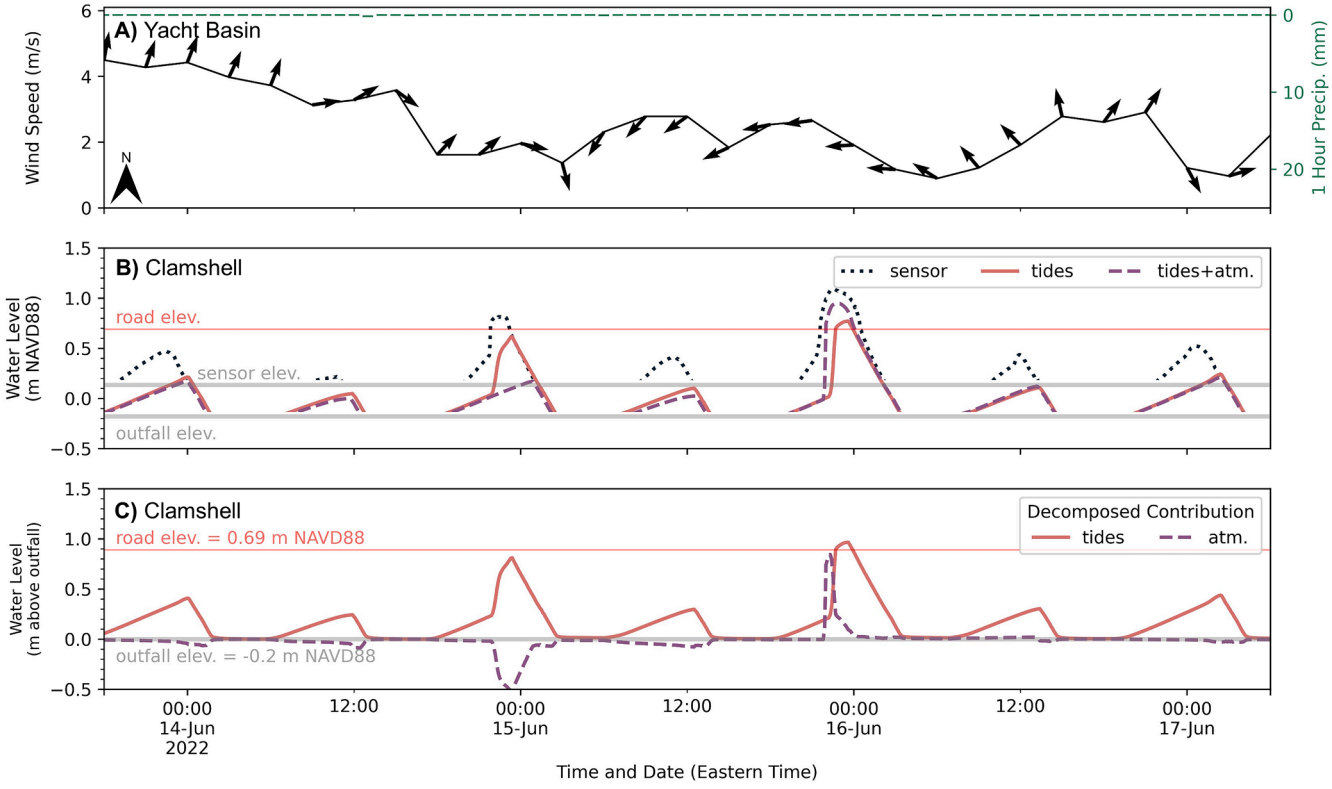

Fig. 4. June 2022 perigean spring tide event. (A) Measured 3-hr wind speed (left y-axis), wind direction (relative to north, arrows), and 1-hr precipitation (right y-axis) in the Yacht Basin. (B) Measured (dotted) and modeled water levels at the Clamshell catch basin from simulations with different model forcing combinations. (C) Decomposition of modeled water levels for tidal (solid line) and atmospheric (dashed line) contributions, relative to the outfall elevation of the Clamshell catch basin. Horizontal lines in (B-C) show elevation of the road (red line), catch basin outfall pipe (gray line), and water level sensor.

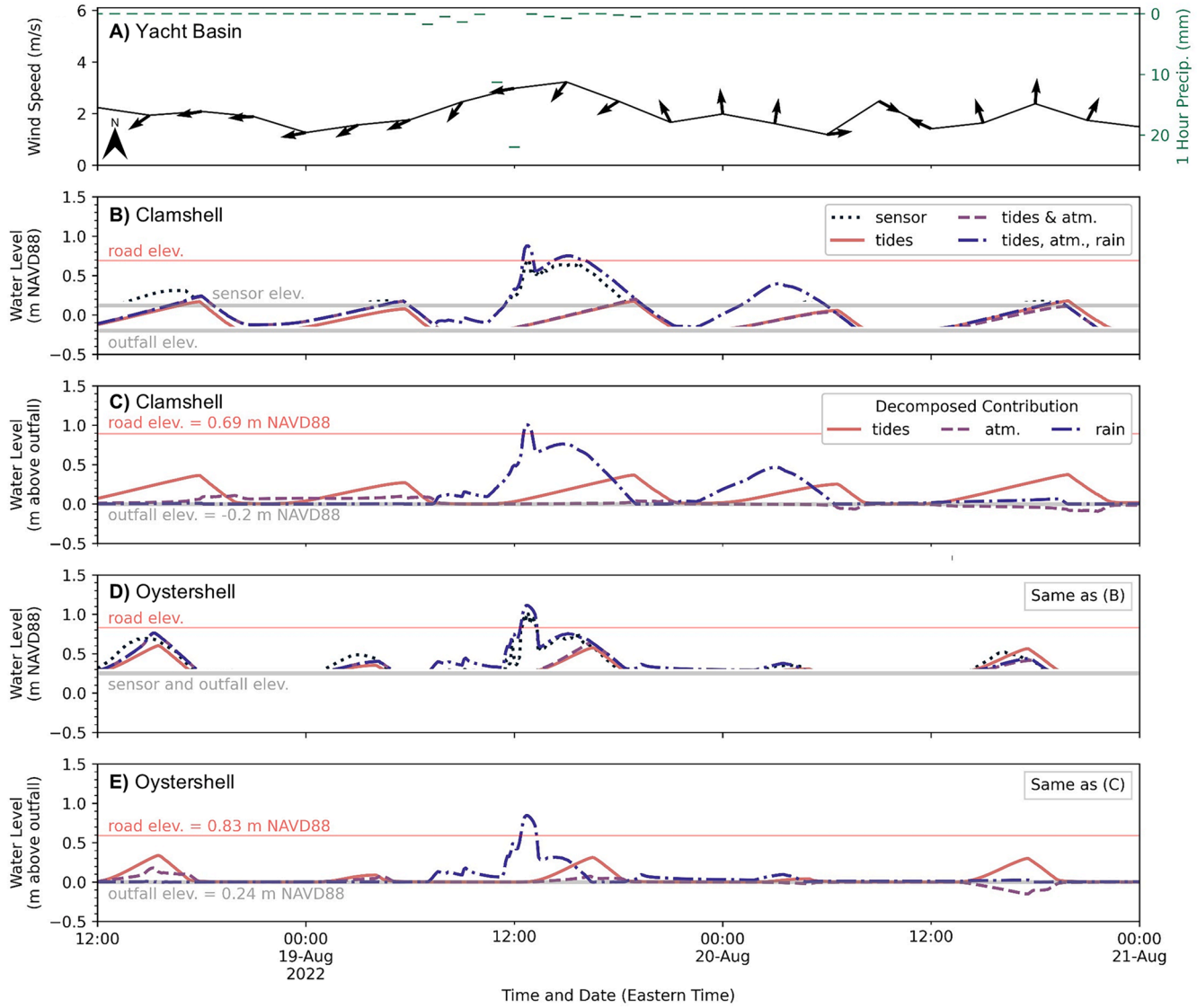

Fig. 5. August 2022 rain event. (A) Measured 3-hr wind speed (left y-axis), wind direction (relative to north, arrows), and 1-hr precipitation (right y-axis) in the Yacht Basin. B,D) Measured (dotted) and modeled water levels at the Clamshell (B) and Oystershell (D) catch basins from simulations with different model forcing combinations. (C,E) Decomposition of modeled water levels for tidal (solid line), atmospheric (dashed line), and rainfall (dash-dot line) contributions, relative to the outfall elevation of the Clamshell (C) and Oystershell (E) catch basins.

tides kept floodwaters on the road by eliminating stormwater drainage capacity.

This compound sequence of three different flood drivers produced the fifth longest flood on record (Fig. 3), longer than would have been expected considering any partial subset of drivers. Rainfall also occurred during the next rising tide on the evening of January 22 (Fig. 6A), but did not produce roadway flooding at either sensor location (Fig. 6B,D) as the tidal amplitude was smaller than the previous tidal peak and atmospheric contributions were small (Fig. 6C,E).

3.2.4. *Flood spatial extents*

The preceding analysis of flood drivers focused on individual sensor locations, where model simulations directly compare to flood measurements. In this section, we use the validated model to look beyond sensor locations and examine how non-tidal drivers compounded with tides to modify the spatial extent of modeled floods. We quantify changes in flood extent as an increase in inundated area and water volume relative to the tides simulations, calculated for the timestep with the maximum modeled flood depth at the Clamshell sensor. We limit our analysis to the north end of the Yacht Basin (in the proximity of the Clamshell sensor, Fig. 7), as this area is subject to both shoreline overtopping and stormwater network inundation.

The decomposition of flood drivers during the June 2022 perigean spring tide event identified that atmospheric forcing (northeasterly winds) compounded with tides to produce roadway flooding at the Clamshell sensor (Fig. 4). This compounding resulted in an increase in inundated area and flood volume, beyond what would have been observed by tides alone, of 4300 m^2 and 1400 m^3 (respectively, seen through comparison of Fig. 7A,B). The contribution from wind setup allows for more overtopping of low-lying shorelines, which then floods the road – first north of the Yacht Basin along Florida Avenue and then along Canal Drive – and increases the connectivity of floodwaters in the road. (The patchiness of floodwaters in Fig. 7A largely stems from flooding via stormwater network inundation by tides.)

The spatial pattern of flooding observed for the other two modeled events differs from the June 2022 perigean spring tide event due to rainfall. For the August 2022 rain event and the January 2023 mixed-drivers event, water accumulates along nearly all roads in this portion of the study site because drainage of rainfall runoff via the stormwater network is impeded by bay water levels that submerge stormwater

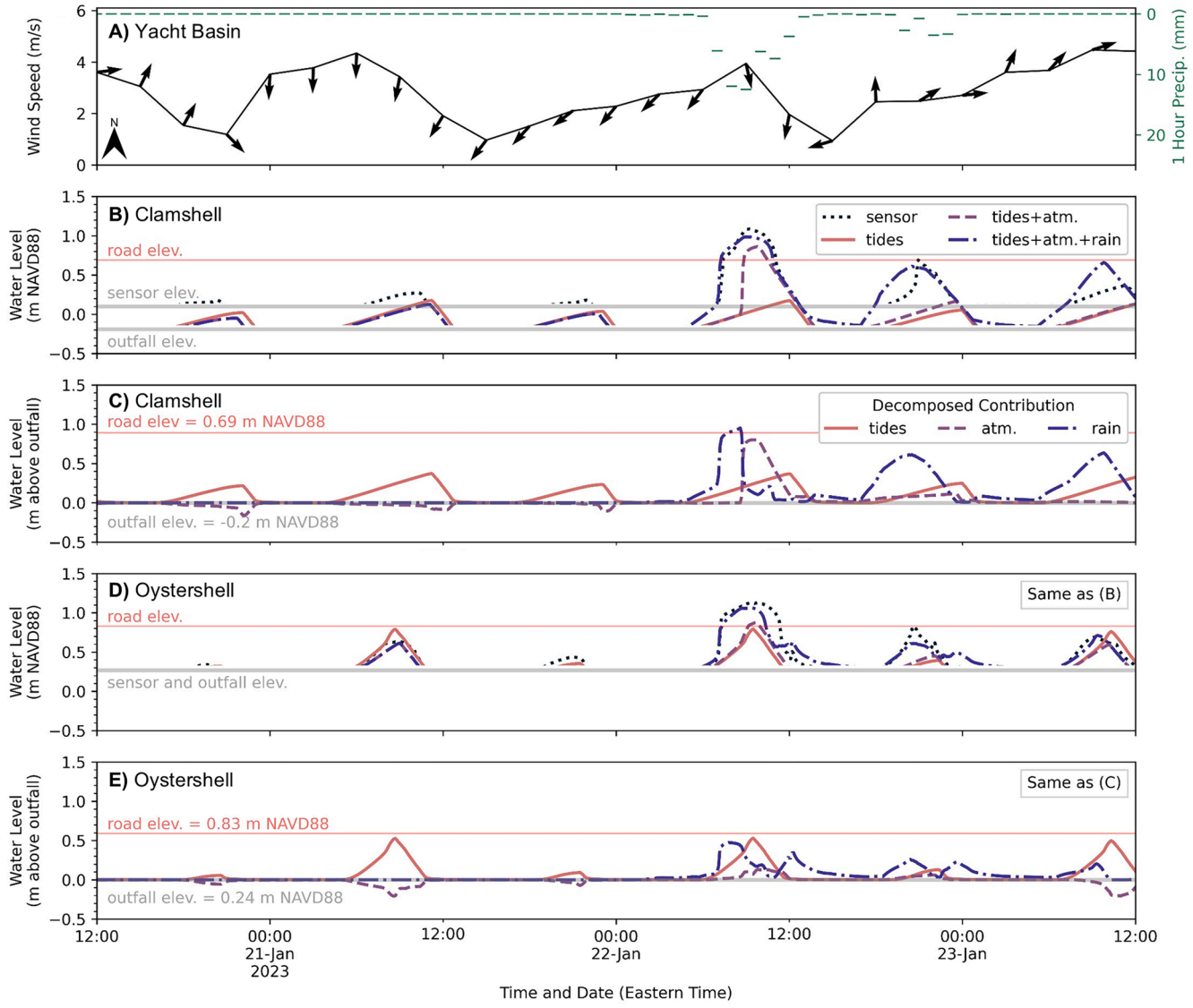

Fig. 6. January 2023 mixed-drivers event. A) Measured 3-hr wind speed (left y-axis), wind direction (relative to north, arrows), and 1-hr precipitation (right y-axis) in the Yacht Basin. B,D) Measured (dotted) and modeled water levels at the Clamshell (B) and Oystershell (D) catch basins from simulations with different model forcing combinations. C,E) Decomposition of modeled water levels for tidal (solid line), atmospheric (dashed line), and rainfall (dash-dot line) contributions, relative to the outfall elevation of the Clamshell (C) and Oystershell (E) catch basins.

outfalls to the Yacht Basin (shown during the time of maximum modeled flood depth at the Clamshell sensor, Fig. 7E,H). Consistent with the findings from the driver decompositions (Figs. 5 and 6), the compound nature of the events resulted in a significant increase in flood volumes beyond what would be expected from tides alone (by 1600 m^3 and 2900 m^3, respectively; Fig. 7E,H).

4. Discussion

In Carolina Beach, NC, we documented 46 floods in one year, highlighting the frequency of floods occurring outside of extreme storms (43 out of 46 floods) due to SLR. Building on the finding of Gold et al. (2023) that rain can compound with even moderate tides to produce coastal flooding due to impaired stormwater networks, we show that other non-tidal factors – namely wind, and the combination of wind, rain, and impaired stormwater networks – contribute to flood magnitude, extent, and duration during tidal floods, and consequently increase the frequency of flooding in low-lying coastal communities (Fig. 8). Important in causing or modulating flooding are both regional-scale marine water level drivers (e.g., tides and wind in Fig. 8) and hyper-local factors like stormwater infrastructure (e.g., backflow prevention devices in Fig. 8), variable shoreline elevations, and rainfall runoff.

In many coastal communities, chronic floods are predicted using tidal forecasts, and therefore floods caused by other drivers can be unexpected. Wind was a major contributor to unexpected flooding in Carolina Beach, and setup from regional winds likely drives similar non-storm flooding in other low-lying coastal communities. During our study period, 33 % of chronic coastal floods (14 of 43 floods, all outside of extreme storms) occurred during forecasted tides below the community's monitoring threshold (Fig. 3D). Eleven of these 14 unexpected floods occurred during a rising or high tide accompanied by northeasterly wind. Wind speeds measured in the Yacht Basin during the unexpected floods were below tropical wind forcing (2.2–6.8 m/s, averaged over the 24 h preceding the event), but as shown in the Supplement (Fig. S.10-S.11), regional winds acting offshore of southeast North Carolina were sufficiently strong (5.2–7.0 m/s in the ADCIRC model, averaged over the 24 h preceding the event) to increase water levels along the open coast by 10–20 cm. This setup from relatively typical wind speeds blowing over an extended fetch, when combined with tides and propagated through tidal inlets, produces roadway flooding. Given

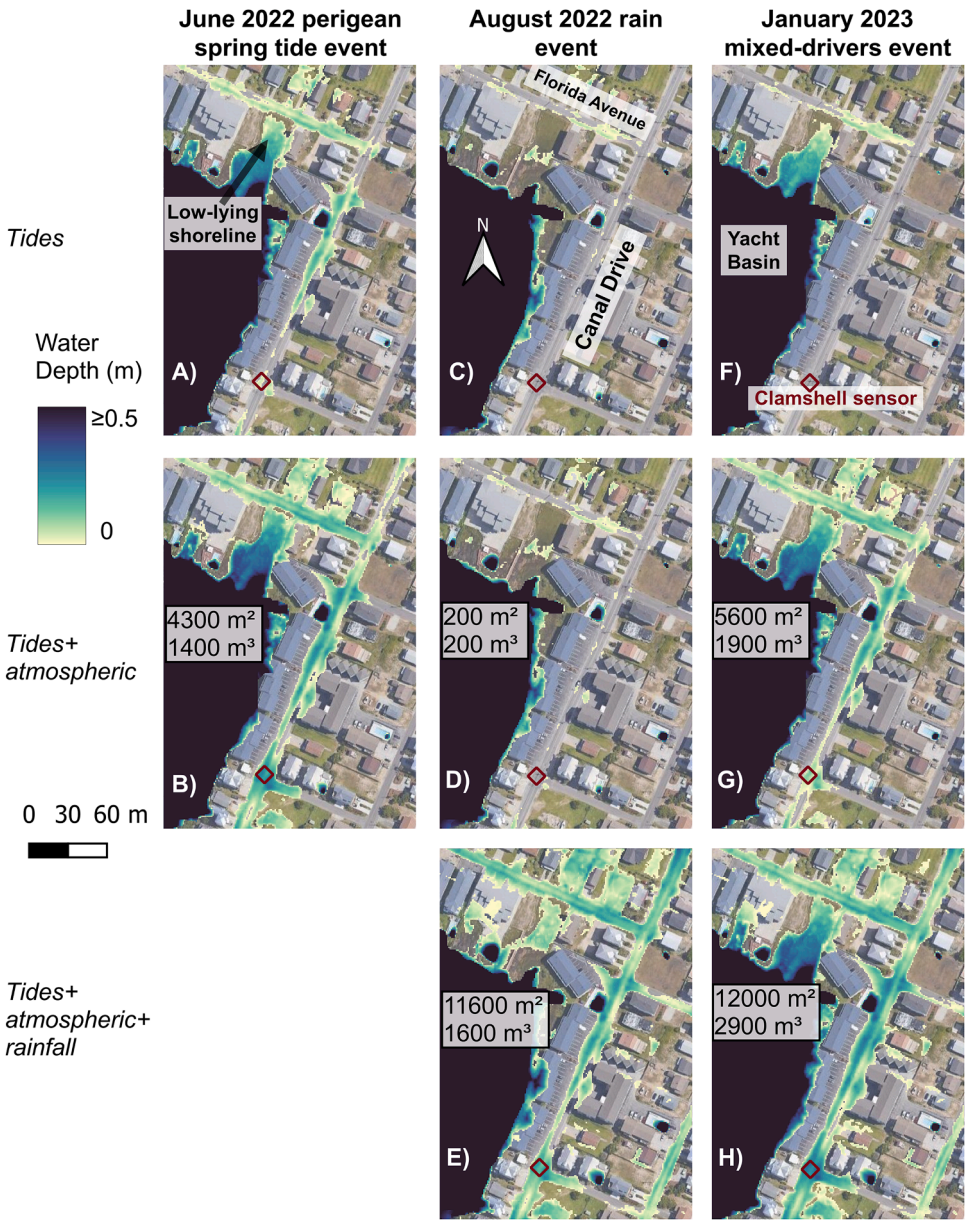

Fig. 7. Simulated maximum flood extents and depths adjacent to the northeast corner of the Yacht Basin (see stormwater system in Fig. 1C). Columns show the three modeled flood events. Rows show the three model flood simulations with different model forcing combinations. Increases in inundated area (m^2; top) and water volume (m^3; bottom) within the plotted extents relative to each event's tides simulation are boxed in the tides + atmospheric and tides + atmospheric + rainfall (expect June 2022, no rain during this event) maps. Flood extents are extracted from the tides + atmospheric + rainfall simulation timestep with maximum modeled flood depth at the Clamshell sensor. A brown diamond indicates the location of the Clamshell sensor.

that non-tidal residuals – which include regional wind setup – have been shown to contribute significantly to marine water levels at tide gauges both in the mid-Atlantic and beyond (e.g., along the US northeast and Gulf coasts; Li et al., 2022), the importance of wind to localized roadway flooding is likely widespread.

Our results build on a growing body of research indicating that flood risk may be substantially underestimated when using simpler models (e.g., Schubert et al. 2024) and point to model coupling (with high-resolution models) as a more appropriate method for modeling of chronic coastal floods. The novel coupling between an ocean-scale hydrodynamic model and a 1D-2D flow model introduced in this paper allows for simulation of flood contributions from marine sources (tides, wind), land-based sources (rainfall), and infrastructure (stormwater, bulkheads) at hyperlocal scales. We find that accurate simulation of flood depths and extents requires resolving stormwater infrastructure, including the effects of backflow prevention devices. The sensitivity of coastal flooding to drainage infrastructure with backflow prevention has been noted previously (e.g., Gallien et al., 2011; 2014), but here we introduce a new method to parameterize the effects of backflow prevention devices by tuning stormwater outfall discharge coefficients (modeled as weirs) to match water levels measured in catch basins (Fig. S.4).

With our validated flood model, we find that wind can increase flood magnitudes, durations (Fig. 4), and spatial extents (Fig. 7B), even during expected perigean spring tide events. Wind and tides can also compound with rainfall to produce floods that are deeper and longer in duration than would have otherwise occurred with individual drivers (Figs. 5 and 6), but flood characteristics (magnitude and duration) vary spatially. The compounding of flood drivers and their interactions that we capture cannot be resolved in bathtub flood models (e.g., Williams and

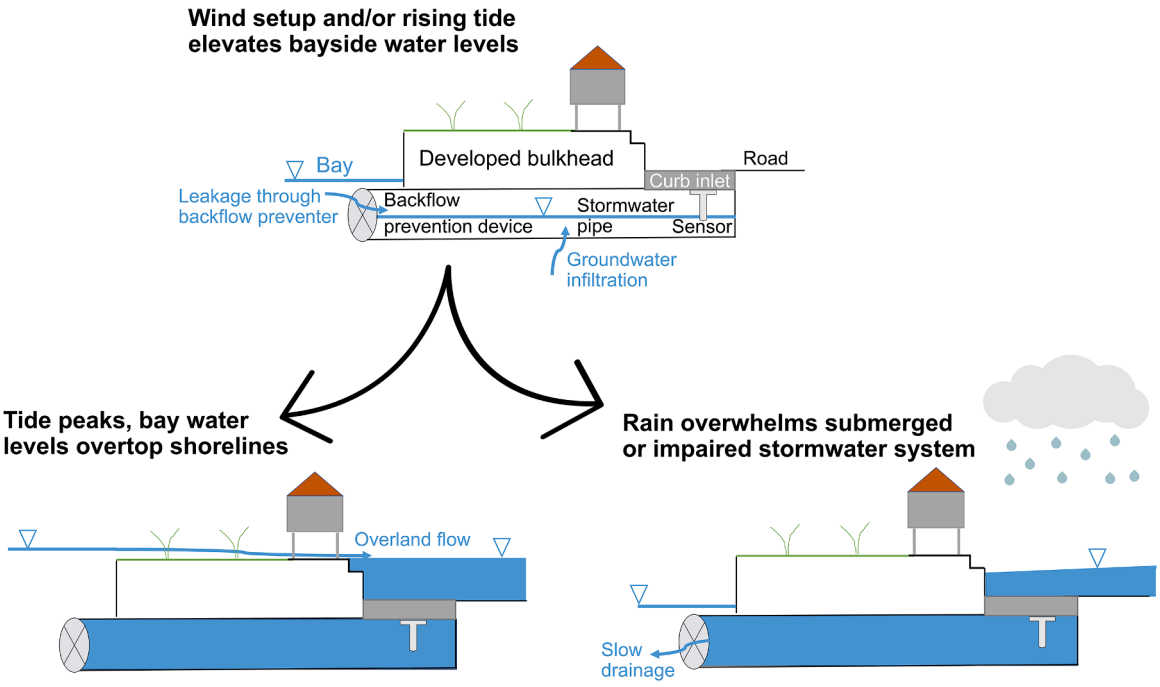

Fig. 8. Illustration of the processes and mechanisms shown herein to contribute to chronic coastal flooding.

Lück-Vogel, 2020; Yunus et al., 2016), nor (non-coupled) hydrodynamic flood models (e.g., Sadler et al., 2020; Shen et al., 2019). Furthermore, the coupled flood model introduced in this study could be extended to include other marine (e.g., wave setup, riverine flow) and land-based processes (e.g., groundwater) that are not currently significant flood drivers in Carolina Beach (see Supplement Section 2), but are suggested as drivers of chronic coastal floods elsewhere (Moftakhari et al., 2017).

For coastal communities facing chronic flooding, considering factors beyond the tidal forecast is critical for effective flood responses and mitigation. In Carolina Beach, 24-hr sustained winds greater than 2.2 m/s (5 mph) out of the northeast often contribute to unexpected floods (Fig. 3D); therefore, flood monitoring could be extended to include forecasts of wind speeds and directions. Wind-driven contributions to flood extent during predicted high-tide events also warrant consideration, as small amounts of wind (from the right direction) can disproportionately enhance flooding in low-lying coastal areas (Fig. 7A-B). Finally, monitoring could be extended to include forecasted rain events, particularly if they occur around tidal peaks. However, monitoring of wind, rain, and tides – as well as the functionality of backflow prevention devices (e.g., biofouling) – presents a significant challenge for local municipalities with limited personnel. Alternatively, flood models, like that presented here, could be adapted to run in a forecast capacity using existing inputs (tidal constituents and forecasted meteorological conditions). Model forecasts could provide spatially continuous predictions of flood depth, extent, and timing to inform community preparedness measures like road closures and alerts. Similarly, in-situ data within stormwater networks could be used during non-flood conditions to track the functionality of backflow prevention devices.

Chronic flooding will become more common in coastal communities worldwide with SLR (IPCC, 2022), and the drivers of these floods will likely change for individual communities; communities that today only flood during the highest high tides may soon need to plan for flooding from wind, rain, and impaired stormwater networks. A local understanding of flood drivers now and in the future is necessary to evaluate the effectiveness of potential flood mitigation strategies. In Carolina Beach, for example, backflow prevention devices installed on stormwater outfalls to the Yacht Basin are effective in preventing small floods from high bay water levels. However, flood prevention is compromised during higher water level events by low-lying shorelines elsewhere (water finds a way) or rainfall occurring at high tide (water has nowhere to go). Larger infrastructure interventions like raising shoreline elevations may change the relative importance of different flood drivers – for example, bulkheads or ring dykes may be effective at reducing flooding from marine-based drivers, but exacerbate flooding from rainfall and groundwater. Stormwater-based interventions like pumps could alleviate rainfall-driven flooding, but may be ineffective against increasing floodwater volumes from overtopping of low-lying shorelines with future SLR.

5. Conclusion

By combining in-situ measurements of flooding and a coupled numerical model, we show that, due to SLR, non-tidal marine (regional wind setup) and land-based factors (rainfall, impaired stormwater networks) lead to flooding at hyperlocal (block-by-block) scales in low-lying coastal communities. These factors can also exacerbate the depth, duration, and extent of (predicted) high-tide floods. Our analysis focuses on the Town of Carolina Beach, NC, USA, which has features that are common to many coastal communities worldwide but is particularly low-lying and therefore a vanguard of what will occur elsewhere with increasing sea levels.

- For low-lying coastal communities exposed to persistent winds blowing over an extended fetch: sustained regional winds – here, greater than 2.2 m/s (5 mph) at the location of flooding or 5.2 m/s offshore – can elevate marine water levels locally during normal tidal cycles and contribute to flooding (modulating flood depths, extents, and durations).
- For communities with stormwater infrastructure at or below the high tide line: partial submergence of stormwater infrastructure (even when equipped with backflow prevention devices) by tides and/or wind setup limits drainage such that even a minor rainstorm – here, 2-hr rain accumulation on the order of 5 to 35 mm – can lead to flooding.
- Models may misrepresent chronic coastal flooding if they do not consider multiple, compounding flood drivers from both regional-

scale marine (e.g., tides and wind) and local-scale land-based (e.g., rainfall runoff) sources interacting with infrastructure (e.g., backflow prevention devices and stormwater pipes/catch basins). Model coupling is an effective method for simulating compounding flood drivers across multiple spatial scales.

Accounting for these additional land and marine-based factors in flood prediction presents challenges for communities with limited capacity to monitor weather and stormwater network performance. Models that can simulate compound interactions between multiple flood drivers and resolve stormwater infrastructure, like the coupled flood model presented here, can build predictive capacity by increasing understanding of flood drivers.

CRediT authorship contribution statement

Thomas Thelen: Writing – review & editing, Writing – original draft, Formal analysis, Data curation. **Katherine Anarde:** Writing – review & editing, Funding acquisition, Conceptualization. **Joel Casey Dietrich:** Writing – review & editing, Conceptualization. **Miyuki Hino:** Writing – review & editing, Funding acquisition, Conceptualization.

Declaration of competing interest

The authors declare that they have no known competing financial interests or personal relationships that could have appeared to influence the work reported in this paper.

Data availability

Flood sensor data are available on our publicly accessible web viewer at the link https://go.ncsu.edu/sunny. Flood model schematization and simulation output files will be made available upon request.

Acknowledgements

This work was supported by Institution Grant (NA22OAR4170109) to the NC Sea Grant Program from the National Sea Grant Office, National Oceanic and Atmospheric Administration. This material is also based upon work supported by the U.S. Department of Homeland Security under Grant Award Number 2015-ST-061-ND0001-01. The views and conclusions contained herein are those of the authors and should not be interpreted as necessarily representing the official policies, either expressed or implied, of the U.S Department of Homeland Security. Anarde was additionally supported by the Gulf Research Program Early-Career Research Fellowship (2000013691-2022). We thank the Town of Carolina Beach staff, especially Jeremy Hardison and Daniel Keating, for their collaboration. We also thank Anthony Whipple, Ryan McCune, Christine Baker, Tomás Cuevas López, Meagan Kittle-Autry, and Julia Harrison for feedback provided during the development of this paper, and Nicolette Volp and Olof Baltus for their guidance during 3Di model development.

Supplementary materials

Supplementary material associated with this article can be found, in the online version, at doi:10.1016/j.watres.2024.122339.

References

APTIM, 2019. Town of Carolina Beach Canal Drive Flooding & Vulnerability Assessment Study. Aptim Coastal Planning & Engineering of North Carolina.

Asher, T.G., et al., 2019. Low frequency water level correction in storm surge models using data assimilation. Ocean Model. 144, 101483 https://doi.org/10.1016/j.ocemod.2019.101483.

Befus, K.M., et al., 2020. Increasing threat of coastal groundwater hazards from sea-level rise in California. Nat. Clim. Change 10, 946–952. https://doi.org/10.1038/s41558-020-0874-1.

Blanton, B.O., Luettich, R.A., 2008. North Carolina Coastal Flood Analysis System Model Grid Generation (No. TR-08-05). RENCI, North Carolina.

Bonnin, G.M., et al., 2004. Precipitation-Frequency Atlas of the United States. Volume 2 Version 3.0. Delaware, District of Columbia, Illinois, Indiana, Kentucky, Maryland, New Jersey, North Carolina, Ohio, Pennsylvania, South Carolina, Tennessee, Virginia, West Virginia. NOAA atlas; 14.

Bosserelle, A.L., et al., 2022. Groundwater rise and associated flooding in coastal settlements due to sea-level rise: a review of processes and methods. Earths Fut. 10, e2021EF002580 https://doi.org/10.1029/2021EF002580.

Buckman, S.T., Sobhaninia, S., 2022. The impact of sea-level flooding on the real estate development community in Charleston SC: results of a ULI member survey. J. Sustain. Real Estate 14, 4–20. https://doi.org/10.1080/19498276.2022.2095699.

Carr, M.M., et al., 2024. Fecal bacteria contamination of floodwaters and a coastal waterway from tidally-driven stormwater network inundation. GeoHealth 8, e2024GH001020. https://doi.org/10.1029/2024GH001020.

Casulli, V., 2009. A high-resolution wetting and drying algorithm for free-surface hydrodynamics. Int. J. Numer. Methods Fluids 60, 391–408. https://doi.org/10.1002/fld.1896.

Casulli, V., Stelling, G.S., 2013. A semi-implicit numerical model for urban drainage systems. Int. J. Numer. Methods Fluids 73, 600–614. https://doi.org/10.1002/fld.3817.

Casulli, V., Stelling, G.S., 2011. Semi-implicit subgrid modelling of three-dimensional free-surface flows. Int. J. Numer. Methods Fluids 67, 441–449. https://doi.org/10.1002/fld.2361.

Dietrich, J.C., et al., 2011. Hurricane Gustav (2008) waves and storm surge: hindcast, synoptic analysis, and validation in Southern Louisiana. Mon. Weather Rev. 139, 2488–2522. https://doi.org/10.1175/2011MWR3611.1.

Dusek, G., et al., 2022. A novel statistical approach to predict seasonal high tide flooding. Front. Mar. Sci. 9.

Fan, Y., et al., 2017. A Coupled 1D-2D hydrodynamic model for urban flood inundation. Adv. Meteorol. 2017, e2819308 https://doi.org/10.1155/2017/2819308.

Gallegos, H.A., et al., 2009. Two-dimensional, high-resolution modeling of urban dam-break flooding: a case study of Baldwin Hills, California. Adv. Water Resourc. 32, 1323–1335. https://doi.org/10.1016/j.advwatres.2009.05.008.

Gallien, T., et al., 2011. Predicting tidal flooding of urbanized embayments: A modeling framework and data requirements. Coast. Eng. 58, 567–577. https://doi.org/10.1016/j.coastaleng.2011.01.011.

Gallien, T., et al., 2014. Urban coastal flood prediction: Integrating wave overtopping, flood defenses and drainage. Coast. Eng. 91, 18–28. https://doi.org/10.1016/j.coastaleng.2014.04.007.

Gold, A., et al., 2023. Data from the drain: a sensor framework that captures multiple drivers of chronic coastal floods. Water Resour. Res. 59, e2022WR032392 https://doi.org/10.1029/2022WR032392.

Gold, A., et al., 2022. Inundation of stormwater infrastructure is common and increases risk of flooding in coastal urban areas along the US atlantic coast. Earth's Fut. 10 https://doi.org/10.1029/2021EF002139 e2021EF002139.

Hague, B.S., et al., 2023. The global drivers of chronic coastal flood hazards under sea-level rise. Earths Fut. 11, e2023EF003784 https://doi.org/10.1029/2023EF003784.

Hauer, M.E., et al., 2023. Sea level rise already delays coastal commuters. Environ. Res. Clim. 2, 045004 https://doi.org/10.1088/2752-5295/acf4b5.

Hayden-Lowe, J., et al., 2022. sunny-day-flooding-project/tutorials: v1.0.1. https://doi.org/10.5281/zenodo.7017187.

Hino, M., et al., 2019. High-tide flooding disrupts local economic activity. Sci. Adv. 5, eaau2736. https://doi.org/10.1126/sciadv.aau2736.

IPCC, Intergovernmental Panel on Climate Change, 2022. Sea Level Rise and Implications for Low-Lying Islands, Coasts and Communities. The Ocean and Cryosphere in a Changing Climate: Special Report of the Intergovernmental Panel on Climate Change. Cambridge University Press, pp. 321–446.

Ju, Y., et al., 2017. Planning for the change: mapping sea level rise and storm inundation in sherman island using 3Di hydrodynamic model and LiDAR. In: Thakuriah, P. (Vonu), Tilahun, N., Zellner, M. (Eds.), Seeing Cities Through Big Data: Research, Methods and Applications in Urban Informatics. Springer Geography. Springer International Publishing, Cham, pp. 313–329. https://doi.org/10.1007/978-3-319-40902-3_18.

Li, S., et al., 2022. Contributions of different sea-level processes to high-tide flooding along the U.S. coastline. J. Geophys. Res. Oceans 127, e2021JC018276. https://doi.org/10.1029/2021JC018276.

Luettich, R.A., et al., 1992. ADCIRC: an advanced three-dimensional circulation model for shelves, coasts, and estuaries. Report 1, Theory and methodology of ADCIRC-2DD1 and ADCIRC-3DL (Report). Coastal Engineering Research Center (U.S.

Macías-Tapia, A., et al., 2021. Effects of tidal flooding on estuarine biogeochemistry: quantifying flood-driven nitrogen inputs in an urban, lower Chesapeake Bay subtributary. Water Res. 201, 117329 https://doi.org/10.1016/j.watres.2021.117329.

Moftakhari, H.R., et al., 2018. What is nuisance flooding? Defining and monitoring an emerging challenge. Water Resour. Res. 54, 4218–4227. https://doi.org/10.1029/2018WR022828.

Moftakhari, H.R., et al., 2017. Cumulative hazard: The case of nuisance flooding. Earths Future 5, 214–223. https://doi.org/10.1002/2016EF000494.

Mydlarz, C., et al., 2024. FloodNet: low-cost ultrasonic sensors for real-time measurement of hyperlocal, street-level floods in New York City. Water Resour. Res. 60, e2023WR036806 https://doi.org/10.1029/2023WR036806.

NOAA, National Oceanic and Atmospheric Administration, 2022. Wrightsville Beach. NC - Station ID, 8658163.

Office for Coastal Management, 2022. 2015-2017 C-CAP Derived 10 meter Land Cover - BETA.
Rogers, E., et al., 2009. The NCEP North American mesoscale modeling system: Recent changes and future plans.
Sadler, J.M., et al., 2020. Exploring real-time control of stormwater systems for mitigating flood risk due to sea level rise. J. Hydrol. 583, 124571 https://doi.org/10.1016/j.jhydrol.2020.124571.
Schubert, J.E., et al., 2024. National-scale flood hazard data unfit for urban risk management. Earth's Future 12, e2024EF004549. https://doi.org/10.1029/2024EF004549.
Seyoum, S.D., et al., 2012. Coupled 1D and noninertia 2D flood inundation model for simulation of urban flooding. J. Hydraul. Eng. 138, 23–34. https://doi.org/10.1061/(ASCE)HY.1943-7900.0000485.
Shen, Y., et al., 2019. Flood risk assessment and increased resilience for coastal urban watersheds under the combined impact of storm tide and heavy rainfall. J. Hydrol. 579, 124159 https://doi.org/10.1016/j.jhydrol.2019.124159.
Silverman, A.I., et al., 2022. Making waves: Uses of real-time, hyperlocal flood sensor data for emergency management, resiliency planning, and flood impact mitigation. Water Res. 220, 118648 https://doi.org/10.1016/j.watres.2022.118648.
Stelling, G.S., 2012. Quadtree flood simulations with sub-grid digital elevation models. Proc. Inst. Civ. Eng. Water Manag. 165, 567–580.
Sweet, W., et al., 2018. Patterns and projections of high tide flooding along the U.S. coastline using a common impact threshold.
Sweet, W., et al., 2022. Global and regional sea level rise scenarios for the United States: updated mean projections and extreme water level probabilities along U.S. coastlines (No. NOAA technical report NOS 01). National Oceanic and Atmospheric Administration. National Ocean Service, Silver Spring, MD.
Thatcher, C.A., et al., 2016. Creating a coastal national elevation database (CoNED) for science and conservation applications. J. Coast. Res. 64–74. https://doi.org/10.2112/SI76-007.
Thiéblemont, R., et al., 2023. Chronic flooding events due to sea-level rise in French Guiana. Sci. Rep. 13, 21695. https://doi.org/10.1038/s41598-023-48807-w.
Volp, N.D., et al., 2013. A finite volume approach for shallow water flow accounting for high-resolution bathymetry and roughness data. Water Resour. Res. 49, 4126–4135. https://doi.org/10.1002/wrcr.20324.
Weather Forecast Office, 2023. Eastern North Carolina Monthly Climate Report. January 2023.
Westerink, J.J., et al., 1992. Tide and storm surge predictions using finite element model. J. Hydraul. Eng. 118, 1373–1390. https://doi.org/10.1061/(ASCE)0733-9429(1992)118:10(1373).
Williams, L.L., Lück-Vogel, M., 2020. Comparative assessment of the GIS based bathtub model and an enhanced bathtub model for coastal inundation. J. Coast. Conserv. 24, 23. https://doi.org/10.1007/s11852-020-00735-x.
Yunus, A.P., et al., 2016. Uncertainties in tidally adjusted estimates of sea level rise flooding (Bathtub Model) for the Greater London. Remote Sens. 8, 366. https://doi.org/10.3390/rs8050366.
Zahura, F.T., Goodall, J.L., 2022. Predicting combined tidal and pluvial flood inundation using a machine learning surrogate model. J. Hydrol. Reg. Stud. 41, 101087 https://doi.org/10.1016/j.ejrh.2022.101087.